International Journal of Impact Engineering 38 (2011) 247–251

Contents lists available at ScienceDirect

International Journal of Impact Engineering

journal homepage: www.elsevier.com/locate/ijimpeng

# Penetration scaling in atomistic simulations of hypervelocity impact

Andrew Higginbotham [a,*], E.M. Bringa [b], Emma A. Taylor [c,1], Giles Graham [d]

[a] Department of Physics, Clarendon Laboratory, University of Oxford, Oxford OX1 3PU, United Kingdom
[b] CONICET and Instituto de Ciencias Basicas, Universidad Nacional de Cuyo, Mendoza CP 5500, Argentina
[c] CEPSAR, The Open University, Walton Hall, Milton Keynes, MK7 6AA, United Kingdom
[d] Mineralogy Department, The Natural History Museum, London SW7 5BD, United Kingdom

ARTICLE INFO

*Article history:*
Received 26 April 2010
Received in revised form
19 August 2010
Accepted 27 October 2010
Available online 3 November 2010

*Keywords:*
Hypervelocity impact
Cratering
Molecular dynamics

ABSTRACT

We present atomistic molecular dynamics simulations of the impact of copper nano particles at 5 km $s^{-1}$ on copper films ranging in thickness from from 0.5 to 4 times the projectile diameter. We access both penetration and cratering regimes with final cratering morphologies showing considerable similarity to experimental impacts on both micron and millimetre scales. Both craters and holes are formed from a molten region, with relatively low defect densities remaining after cooling and recrystallisation. Crater diameter and penetration limits are compared to analytical scaling models: in agreement with some models we find the onset of penetration occurs for $1.0 < f/d_p < 1.5$, where $f$ is the film thickness and $d_p$ is the projectile diameter. However, our results for the hole size agree well with scaling laws based on macroscopic experiments providing enhanced strength of a nano-film that melts completely at the impact region is taken into account.



## 1. Introduction

A detailed understanding of cratering mechanisms and morphologies resulting from hypervelocity impact is critical for analysis of experiments such as Stardust. Post-flight examinations of retrieved space hardware frequently show evidence of micro-cratering as a result of collisions with micrometeoroids/interplanetary dust particles [1,2]. Laboratory simulations using light-gas-guns (LGG) have typically been used to generate analogue impact features [3]. These simulations enable insights into the micro-cratering processes including residue preservation and the ability to calibrate the original projectile size. To support the interpretation of impact craters preserved on the aluminium foils on the collection tray assembly of NASA's STARDUST cometary sample return spacecraft [4], a detailed LGG shot program was performed to calibrate particle size from craters down to approximately 1 μm in diameter [5]. During the preliminary STARDUST post-flight investigation of the foils, a diverse range of crater diameters were observed from a few hundred μm down to tens of nm [6]. The observation of the abundant nm-sized craters requires further laboratory analogue impacts. However, at this size regime there are operational difficulties using LGG facilities, therefore different methods are required.

For macroscopic impactors ($d_p > 1$ μm) impacts can be carried out experimentally using light-gas-guns (but there are limitations on the nature and type of particles that can be accelerated to a given velocity). However, there are currently limited experimental techniques able to easily access the sub-micron regime, with only a handful of experiments using projectiles of hundreds of nanometers. Simple empirical scaling laws extrapolated to the nanometer regime do not seem to predict crater sizes for nano particles with dozens to thousand of atoms [7].

In this paper we investigate cratering due to a fully dense copper projectile undergoing hypervelocity impact with a single crystal copper film. We show that penetration occurs at a similar particle radius to film thickness ratio as in macroscopic impacts. We also discuss the applicability of macroscopic scaling equations in this regime.

In Section 2 we describe the simulations and analysis techniques employed. Discussion of the results in both the penetration and cratering regimes is presented in Section 3.

## 2. Simulations

Simulations were carried out using non-equilibrium molecular dynamics (NEMD). This technique determines material response of an ensemble of atoms by integration of Newton's equations based

* Corresponding author.
*E-mail address:* andrew.higginbotham@physics.ox.ac.uk (A. Higginbotham).
[1] Permanent address: MMI Engineering, The Brew House, Wilderspool Park, Greenall's Avenue, Warrington, Cheshire WA4 6HL, United Kingdom.

0734-743X/$ – see front matter © 2010 Elsevier Ltd. All rights reserved.
doi:10.1016/j.ijimpeng.2010.10.034

**Notation**

| | |
|---|---|
| $d_d$ | Crater depth |
| $d_c$ | Crater diameter |
| $d_h$ | Diameter of hole at rear target surface |
| $\rho_t$ | Film density |
| $f$ | Film thickness |
| $\rho_p$ | Projectile density |
| $d_p$ | Projectile diameter |
| $\sigma_t$ | Yield stress of target |

on a semi-empirical interatomic potential. In this case the Mishin copper potential was chosen [8]. This potential is fitted to the equation of state of Cu, and gives good energetics for defects. The melting temperature for this potential is approximately 1200 K. Previous work has also shown that this potential is able to reliably recreate high pressure, high strain rate behaviour in single crystal [9] and polycrystalline samples [10]. Note that this technique describes the interaction of distinct atoms it allows the study of nanoscale systems in a way not accessible to hydrocodes, where mesh entangling and difficulties in treating microstructure at the nanoscale inhibit meaningful simulation.

A spherical projectile, $d_p = 4$ nm, (containing close to 3000 atoms), was allowed to impact at normal incidence into a free standing, thin, single crystal copper film at a velocity $V = 5$ km s$^{-1}$. The initial temperature of both impactor and substrate was 5 K with sample thermalised (in the microcanonical ensemble [11]) for several picoseconds before impact. This temperature was chosen to simplify visual analysis of the samples, however, simulations at 300 K showed quantitatively similar features. After impact the system was allowed to evolve until the crater morphology had stabilised. Hole and crater dimensions within 10% of the final values were typically reached 40–50 ps after impact, but simulations were run for a total of 130 ps to ensure that the late structural relaxation did not modify the relevant dimensions.

The films were square, with a side length of 36 nm, leading to samples with 110,650 atoms per nm of film thickness. Periodic boundary conditions were imposed at the edges of the film. Thickness of the film was varied between 2 nm and 16 nm. The size of the craters did not change (within our error bars) when the size of the simulation cell was doubled (leading to a 72 nm foil width), indicating that periodic boundary constraints did not significantly affect crater formation mechanisms.

Simple analysis was carried out by visualisation of the impact process. The centrosymmetry parameter (csp) was used as an indicator of local structure in the initially perfect crystal. The csp of an atom, i, in an fcc crystal is defined as [12] –

$$P = \sum_{j=1\ldots6} |\mathbf{R}_j + \mathbf{R}_{j+6}|^2$$

where $\mathbf{R}_j$ and $\mathbf{R}_{j+6}$ are the position vectors of the 12 nearest neighbours of atom i. The indexing is defined such that $\mathbf{R}_j + \mathbf{R}_{j+6} = 0$ for a perfect crystal; that is to say $\mathbf{R}_j$ and $\mathbf{R}_{j+6}$ have positions related by in inversion about $\mathbf{R}_i$ for all $j = 1\cdots6$. If the atoms around $i$ move from their lattice positions, atom i's csp will increase. This leads to a measure of the departure from centrosymmetry useful for diagnosing both defects and amorphous phases resulting from melting.

## 3. Results

The thin film hypervelocity simulations presented show surprising qualitative and quantitative similarities to macroscale impact experiments. Fig. 1 shows the impact and subsequent cratering or penetration for $0.5 \leq f/d_p \leq 4$. It can be seen that the final crater morphology is broadly similar to those seen experimentally [6,13,14]. There is a clear crater rim for $f = 16$ nm, but curling lips are only observed for larger projectiles [15].

In the limit of small thickness, (i.e. small $f/d_p$), we observe penetration of the projectile, as expected. For $f = 2$ and $f = 4$ nm the early frames show void nucleation in a molten region, similar to the initial stages of spall in a liquid [16,17]. This mechanism is similar to that seen during the collision of nanograins by Ohnishi et al. [18]. Note that this molten region covers the entire thickness of the film. This melting dominated behaviour explains why we saw very little difference between 10 and 300 K simulations; both temperatures are significantly below melting.

The film expands and breaks apart in elongated fragments, which slowly evolve into more spherical shapes due to surface tension. As most of the hot molten material is shed away, the remaining film displays a thin molten covering at the side of the hole, surrounded by defects (point defects, line defects - dislocations, and planar defects - stacking faults and twin boundaries). Only a few defects survive the cooling and recovery stage and are shown as red lines in the final frame.

At $f = 6$ nm ($f/d_p = 1.5$) we observe no penetration. The film melts throughout its entire thickness, but the additional surrounding material allows faster cooling and momentum transfer avoiding perforation. The large dislocation density produced in {111} planes, seen at 45° respect to the impact direction, is mostly recovered and leads to a perfect crystal with few defects around the crater. The dislocation density, however, is larger than in the thinner films, since the surface is less effective as a defect sink.

The computational expense of these simulations (around 3600 cpu-hours each) prevents a more detailed examination of parameter space. It is clear however that the onset of penetration occurs for $1.0 < f/d_p < 1.5$. We transition from a region of full penetration ($d_h = d_c$) at $f/d_p = 1.0$ to a cratering regime ($d_h = 0$) at $f/d_p = 1.5$.

Numerous penetration limit equations of varying complexity exist to predict the onset of the penetration regime. Table 1 lists a selection of these equations. The Cour–Palais equation [19] is a simple expression with no dependence on material strength. McDonnell et al. [20] use a more complex model to predict the foil thickness which satisfies the condition $f = d_c$ at the penetration limit. The equation in Gardner et al. [21] was fitted to describe the perforation region and so gives the condition of $d_h = 0$. Although Cour–Palais fails to predict a reasonable penetration limit for the nanoscale impacts it is seen that there is reasonable agreement between the simulations and the predictions of Gardner and of McDonnell.

A more general form of the equation presented in Gardner et al. describes the scaling of hole diameter –

$$\frac{d_p}{f} = A\left(\frac{10}{9+\exp\left(\frac{d_h}{fB}\right)}\right) + \frac{d_h}{f}\left(1-\exp\left(-\frac{d_h}{fB}\right)\right) \quad (1)$$

where

$$A = 6.97\left(\frac{V\rho_p}{\sqrt{\sigma_t\rho_t}}\right)^{-0.723}\left(\frac{\sigma_t}{\sigma_{Al}}\right)^{-0.217} f^{-0.053} \quad (2)$$

and

$$B = B_1 + B_2 V \quad (3)$$

$d_p$ and $f$ have units of microns. For Cu, $B_1 = 3.2$ and $B_2 = 2.62$ [21]. We must use a suitable yield stress in this equation. Gardner et al. suggest a yield stress of 0.22 GPa for copper, a value consistent with

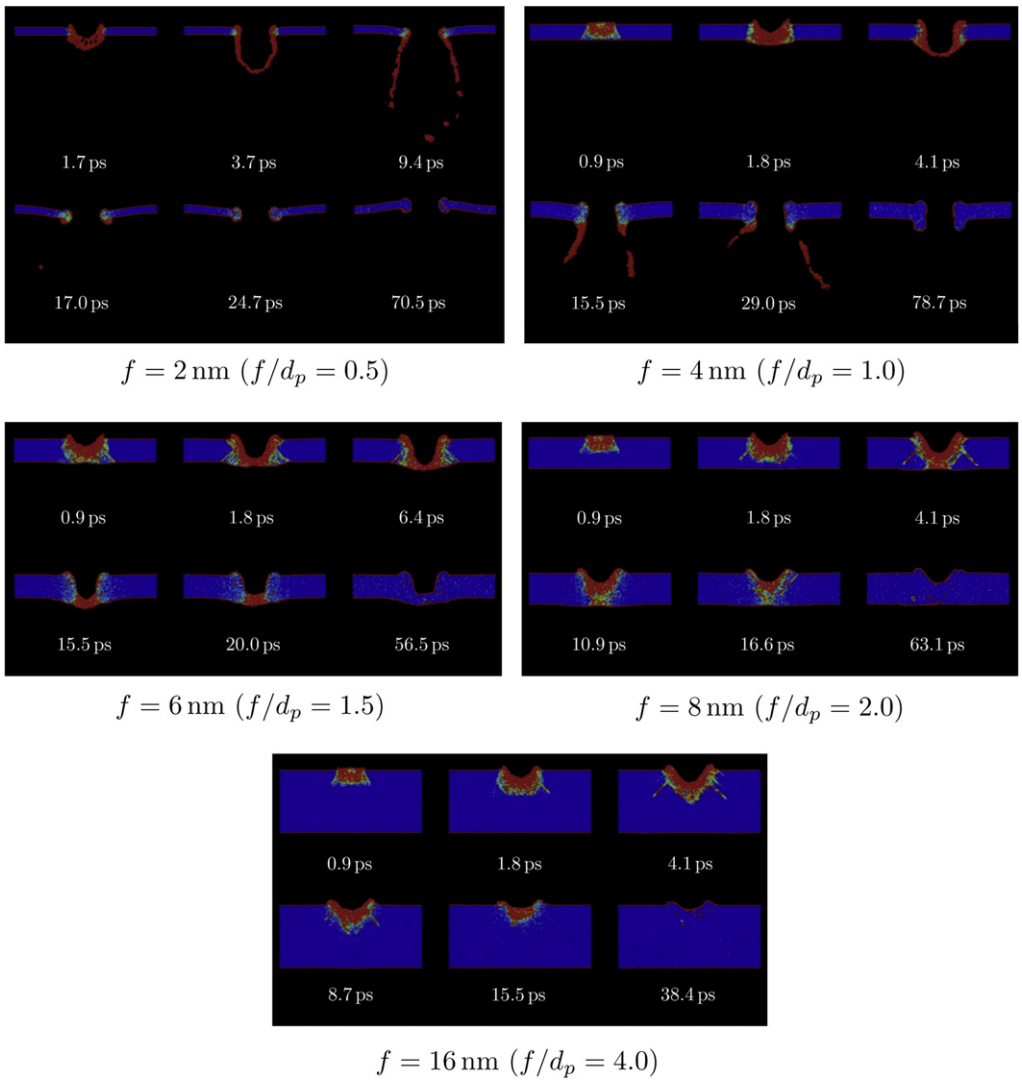


**Fig. 1.** Color online: Snapshots showing evolution of the crater for $0.5 \leq f/d_p \leq 4$. Color denotes centrosymmetry parameter; a measure of order in the crystal structure. Blue indicates perfect crystal with red denoting highly discovered environments. (For interpretation of the references to colour in this figure legend, the reader is referred to the web version of this article).

those measured in polycrystalline copper samples. However, this is significantly lower than yield stresses derived from molecular dynamics calculations of shock induced plasticity in single crystal copper where stresses of just over 30 GPa are required to induce plastic flow [9]. This number is known to be significantly higher than most polycrystalline experimental values due to high strain rate effects, and the lack of pre-existing defects and defect sources, necessitating homogeneous nucleation of dislocations to yield plastically.

The predicted crater width in the penetration regime is plotted for both 0.22 and 30 GPa in Fig. 2, alongside the data from our MD simulations. It is seen that the 30 GPa curve significantly underestimates the crater size. However, this can be easily understood by noting that we see melt throughout the entire thickness of the foil prior to perforation. This suggests that a more pertinent yield stress to use would be a measure of strength (at ultra-high strain rate) in the molten material. One measure of yield strength in this regime is the spall strength [17,22]. It should be remembered that early stages

**Table 1**
A selection of penetration limit equations and the predicted minimum foil thickness for penetration of a 4 nm diameter projectile at 5 km $s^{-1}$. Units for Cour–Palais and McDonnell are cgs with V in km $s^{-1}$. Gardner is in SI units with $d_p$ in μm. Values used are: $\rho_{Fe} = 7.874$ g $cm^{-3}$; $\rho_{Al} = 2.78$ g $cm^{-3}$; $\rho_{Cu} = 8.95$ g $cm^{-3}$; $\sigma_{Al} = 0.069$ GPa; $\sigma_{Cu} = 0.22/30$ GPa. We give values for strength 0.22 and 30 GPa if the equation is strength dependent.

| | | |
|---|---|---|
| Cour–Palais [19] | $\frac{f_{\max}}{d_p} = 0.65 d_p^{0.056} \rho_p^{0.52} V^{0.875}$ | $\frac{f_{\max}}{d_p} = 3.64$ |
| McDonnell and Sullivan [20] | $\frac{f_{\max}}{d_p} = 1.272 d_p^{0.056} \left(\frac{\rho_p \rho_{Al}}{\rho_t \rho_{Fe}}\right)^{0.476} \left(\frac{\sigma_{Al}}{\sigma_t}\right)^{0.134} V^{0.806}$ | $\frac{f_{\max}}{d_p} = 1.06/0.55$ |
| Gardner et al. [21] | $\frac{f_{\max}}{d_p} = 0.129 \left(\frac{V \rho_p}{\sqrt{\sigma_t \rho_t}}\right)^{0.763} \left(\frac{\sigma_t}{\sigma_{Al}}\right)^{0.229} d_p^{0.056}$ | $\frac{f_{\max}}{d_p} = 1.73/0.82$ |

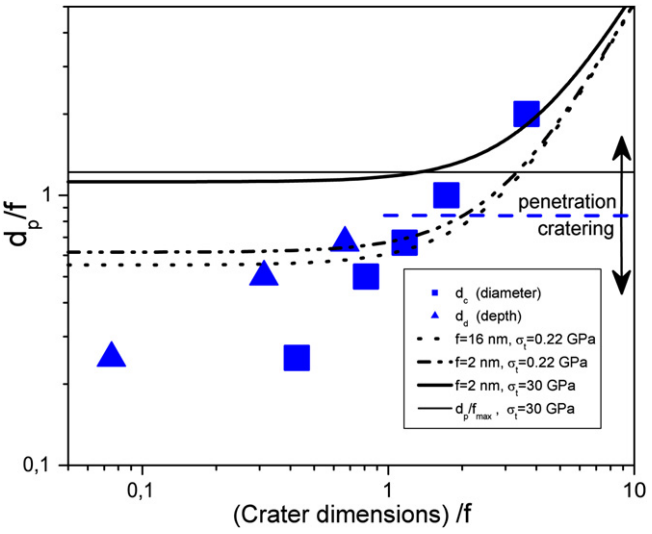


**Fig. 2.** Color online: Scaled crater dimensions as a function of scaled particle diameter. The crater diameter and depth are shown and compared to the Gardner et al. [21] macroscopic scaling law for crater diameter assuming a number of yield strengths and film thicknesses. We also include a thick dashed line indicating the boundary between penetration and cratering regimes in our simulations.

of the perforation process resemble liquid spall so this may be a suitable choice of yield criterion.

Luo et al. present results for spall strength in Mishin copper at strain rates comparable to the present study [16]. They observe spall strength of 13.9 GPa for an impact velocity of 2 km $s^{-1}$ on a 10 K sample. They also report the spall strength falling as a function of impact velocity. If one assumes that the Gardner scaling holds at the micro-scale this would imply a yield strength of between 2 and 5 GPa for our 5 km $s^{-1}$ impacts. This suggests that a liquid spall strength (or a similar quantity) may be a more suitable yield stress in the case of melt-dominated micro-cratering processes.

From scaling of macroscopic results it would be expected that with increasing $f/d_p$ we should transition to the cratering regime via a marginal perforation region where a small hole of diameter $d_h < d_c$ opens on the rear surface, as a result of spallation in the target. In macroscopic targets, spall due to large tensile stress is typically linked to the presence of pre-existing defects, like inclusions, grain boundaries, microfractures, which are not included in our simulations. Therefore, it is not surprising that back-spallation is not observed here. Of course, the small thickness of the sample may also be inhibiting such processes.

For $f/d_p \geq 1.5$ the simulations show a cratering regime where formation mechanisms are again dominated by melting. The subsequent recrystallisation of target and projectile material leads to a healing of the crater prior to cooling of the target. This ability of the crater to recrystallise allows accommodation of deformation leading to a crater with relatively little plastic deformation.

Fig. 1 shows three simulations in the cratering regime for $f = 6$, 8 and 16 nm. The crater size for these film thicknesses is the same as that found in preliminary simulations of semi-infinite targets. The crater depth increases roughly linearly with $d_p/f$.

## 4. Discussion and conclusions

We have carried out perforation and cratering simulations at the atomic level. We have used projectiles with a diameter of 4 nm and film thickness of 0.5–4 times the projectile diameter. Penetration occurs for a film thickness equal or smaller than the projectile diameter, i.e. $f/d_p$ in the range 1–1.5. This agrees roughly with a number of extant scaling laws fitted to macroscale impacts, as shown in Table 1.

Independently of penetration, we observe a nearly constant crater/hole diameter, about twice the projectile diameter. As shown in Fig. 2, empirical scaling laws, obtained from experiments at the micron-cm scale, seem to agree with our simulations, if we use the nominal experimental strength for Cu. This is similar to the work from Samela et al., [23] which used an experimental value of strength to fit MD results of crater size. However, this is not an appropriate comparison, because one should use the simulated MD material strength to obtain consistent values. In fact, the macroscopic scaling laws do not follow our simulations when using simulated strength values, indicating that they might break in experiments at the nanoscale.

This problem was discussed from a different angle by Walsh et al., [24] which pointed out that for sub-micron projectiles, the large resulting strain rate might increase significantly the yield strength of the material. This reasoning is supported by measurement of material strength under shock conditions [25] and by Walsh cratering data. In our simulations, the strain rate is extremely high (above $10^{12}$ $s^{-1}$) in the early stages of crater formation, so the reasoning by Walsh and co-workers would apply. Since our samples are perfect single crystals we would also expect to have higher strength than in most experimental conditions. However, in our simulations, a detailed analysis of material strength is complicated because the cratering process is dominated by melt.

We note that the scale of the craters under consideration is considerably smaller than typical grain sizes (tens of microns) so the single crystal assumption is actually well justified, but real single crystals will have defects such as dislocations, microcracks, and impurities which might change strength, melting nucleation and recrystallization. If cratering happens near such defects, our results would change. Simulations in films with defects will need to be carried out in the future. We also note that our simulations are for a ductile metallic film. Oxide films might display a different behavior, for instance leading to brittle fracture and changing penetration thresholds. On the other hand, a calculation of when the melting of the whole thin film occurs, given the thermal properties of the target, might provide an estimate of the onset of penetration for both metals and oxide films.

Given that melting plays a fundamental role in crater formation in our simulations, it is reasonable to expect that the film temperature would affect penetration and crater dimensions for temperatures closer to melt. However, film temperature does not appear in any of the macroscopic scaling laws considered here. Simulations at different temperatures are needed to explore this further. Experiments looking at cratering at low/high temperatures might also provide much needed information.

"Stardust" results have found sub-micron craters as a result of cometary dust bombardment and novel nanotechnology techniques and astrophysically relevant experiments may soon explore impact experiments with projectiles in the nanometer scale, opening up a new window on penetration processes [26].

## References

[1] Brownlee DE, Joswiak D, Bradley J, and Hrz F. Interplanetary meteoroid debris in ldef metal craters. LDEF - *69 months in Space Second Post-Retrieval Symposium, NASA CP-3194 Part 2*., pages 577–584, 1993.
[2] Graham GA, Kearsley AT, Grady MM, Wright IP, McDonnell JAM. The collection of micrometeoroid remnants from low earth orbit. Advances in Space Research 2000;25(2):303–7. Sample Return Missions to Small Bodies.
[3] Burchell MJ, Cole MJ, McDonnell JAM, Zarnecki JC. Hypervelocity impact studies using the 2 mv van de graaff accelerator and two-stage light gas gun of the university of kent at canterbury. Measurement Science and Technology 1999;10(1):41–50.

[4] Brownlee DE, Tsou P, Anderson JD, Hanner MS, Newburn RL, Sekanina Z, et al. Stardust: comet and interstellar dust sample return mission. Journal of Geophysical Research 2003;108:8111.
[5] Kearsley AT, Burchell MJ, Horz F, Cole MJ, Schwandt CS. Laboratory simulation of impacts on aluminum foils of the stardust spacecraft: calibration of dust particle size from comet wild-2. Meteoritics & Planetary Science 2006;41.
[6] Horz Friedrich, Bastien Ron, Borg Janet, Bradley John P, Bridges John C, Brownlee Donald E, et al. Impact features on stardust: implications for comet 81P/Wild 2 dust. Science 2006;314(5806):1716–9.
[7] Christian Anders, Gerolf Ziegenhain, Steffen Zimmermann, Herbert M. Urbassek. Cluster-induced crater formation. Nuclear Instruments and Methods in Physics Research Section B: Beam Interactions with Materials and Atoms 2009;267(18). In: Tianmin Wang, Fei Gao, Wangyu Hu, Wensheng Lai, Guang-Hong Lu, Xiaotao Zu, Editors. Proceedings of the ninth international conference on computer simulation of radiation effects in solids, 15 September 2009. p. 3122–3125.
[8] Mishin Y, Mehl MJ, Papaconstantopoulos DA, Voter AF, Kress JD. Structural stability and lattice defects in copper: ab initio, tight-binding, and embedded-atom calculations. Physical Review B May 2001;63(22):224106.
[9] Bringa EM, Cazamias JU, Erhart P, Stölken J, Tanushev N, Wirth BD, et al. Atomistic shock Hugoniot simulation of single-crystal copper. Journal of Applied Physics 2004;96:3793.
[10] Bringa Eduardo M, Caro Alfredo, Wang Yinmin, Victoria Maximo, McNaney James M, Remington Bruce A, et al. Ultrahigh strength in nano-crystalline materials under shock loading. Science 2005;309(5742):1838–41.
[11] Allen MP, Tildesley DJ. Computer simulation of liquids. New York, NY, USA: Clarendon Press; 1989.
[12] Kelchner CL, Plimpton SJ, Hamilton JC. Dislocation nucleation and defect structure during surface indentation. Physical Review B 1998;58(17):11085–8.
[13] Valerio-Flores O, Murr L, Hernandez V, Quinones S. Observations and simulations of the low velocity-to-hypervelocity impact crater transition for a range of penetrator densities into thick aluminum targets. Journal of Materials Science 2004;39:6271–89.
[14] Esquivel EV and Murr LE. Grain boundary contributions to deformation and solid-state flow in severe plastic deformation. Materials Science and Engineering: A 2005;409(1-2):13–23. Micromechanics of Advanced Materials II - TMS 2005 Annual Meeting, in Honour of James C.M. Li's 80th Birthday.
[15] Bringa EM. Unpublished.
[16] Luo Sheng-Nian, An Qi, Germann Timothy C, Han Li-Bo. Shock-induced spall in solid and liquid cu at extreme strain rates. Journal of Applied Physics 2009;106(1):013502.
[17] Grady DE. The spall strength of condensed matter. Journal of the Mechanics and Physics of Solids 1988;36(3):353–84.
[18] Ohnishi N, Bringa EM, Remington BA, Gilmer G, Minich R, Yamaguchi Y, et al. Numerical analysis of nanograin collision by classical molecular dynamics. Journal of Physics: Conference Series 2008;112(4):042017. 4pp.
[19] Cour-Palais BG. Space vehicle shielding design. Proc. Comet Halley Micrometeroid Hazard Workshop, ESA SP-153:85–92, 1979.
[20] McDonnell JAM, Sullivan K. Hypervelocity impacts on space detectors: decoding the projectile parameters. Hypervelocity impacts in spaceunit for space sciences. Canterbury: University of Kent; 1992. 3947.
[21] Gardner DJ, McDonnell JAM, Collier I. Hole growth characterisation for hypervelocity impacts in thin targets. International Journal of Impact Engineering 1997;19(7):589–602.
[22] Kanel GI, Razorenov SV, Baumung K, Singer J. Dynamic yield and tensile strength of aluminum single crystals at temperatures up to the melting point. Journal of Applied Physics 2001;90(1):136–43.
[23] Samela Juha, Nordlund Kai. Atomistic simulation of the transition from atomistic to macroscopic cratering. Physical Review Letters Jul 2008;101(2)(027601).
[24] Walsh JM, Stradling GL, Idzorek GC, Shafer BP, -DO WX, Curling Jr HL. Microparticle impacts at ultra-high velocities: their relation to macroparticle impacts. International Journal of Impact Engineering 1993;14(1–4):775–84.
[25] Murphy WJ, Higginbotham A, Kimminau G, Barbrel B, Bringa EM, Hawreliak J, et al. The strength of single crystal copper under uniaxial shock compression at 100 gpa. Journal of Physics: Condensed Matter 2010;22(6):065404. 5pp.
[26] Leroux H, Stroud RM, Dai ZR, Graham GA, Troadec D, Bradley JP, et al. Transmission electron microscopy of cometary residues from micron-sized craters in the stardust al-foils. Meteoritics Planetary Science 2008;43:143–60.